Journal of Engineering Science and Technology
24th EURECA 2025 Special Issue April (2026) 31 - 42

DUAL-BAND MICROSTRIP ANTENNA FOR 5G APPLICATIONS

INTAN IZAFINA IDRUS[1,*], NOHAIDDA SARIFF[1], ABDUL WAJID HAMZA[1], MANEE SANGARAN DIAGARAJAN[1], KIAN LUN SOON[1], YOSHIHIDE YAMADA[2], PUTERI NOR AZNIE FAHSYAR[3]

[1]School of Engineering, Taylor's University, Taylor's Lakeside Campus,
No. 1 Jalan Taylor's, 47500, Subang Jaya, Selangor DE, Malaysia
[2]Department of Electronic Systems Engineering, Malaysia-Japan International Institute of Technology, Kuala Lumpur, Malaysia
[3]Higher College of Technology, Abu Dhabi UAE
*Corresponding Author: intanizafina.idrus@taylors.edu.my

Abstract

The rapid deployment of sub-6 GHz 5G mobile communication system has increased the need for compact and low-cost antennas with dual-band operation. Conventional microstrip antennas typically operate at a single frequency band and suffer from limited bandwidth. Moreover, the literature reports that many dual-band antenna designs rely on complex structures, which lead to high fabrication cost. A compact dual-band microstrip antenna based on a single-layer structure operating at two frequency bands of 3.6 GHz and 5.4 GHz for sub-6 GHz 5G applications is presented in this paper. Initially the single-band microstrip antenna is designed using transmission-line model equations to excite the fundamental TM_{10} mode at 3.6 GHz. Operation of the dual-band is achieved by introducing stub and slot loading techniques, which generate a second resonance corresponding to the TM_{11} mode at 5.4 GHz. The incorporation of quarter-wavelength stub and slots on the single-band microstrip antenna and ground plane enables dual-band operation while maintaining structural simplicity. A low-loss substrate material named NPC-F220A is used to design microstrip antenna with single and dual bands. The designed antennas are simulated using CST Studio Suite software. The overall dimensions of the proposed dual-band microstrip antenna are $50 \times 42 \times 0.289$ mm^3. The return losses are −35.7 dB and −13.7 dB at 3.6 GHz and 5.4 GHz, respectively. The gain of the antenna is 6.2 dBi and 5.9 dBi at 3.6 GHz and 5.4 GHz, respectively. The radiation patterns exhibit good symmetry at boresight at both frequencies of 3.6 GHz and 5.4 GHz. The results demonstrate that the proposed dual-band microstrip antenna is suitable for sub-6 GHz 5G applications.

Keywords: 5G applications, Dual-band, Loading, Sub-6 GHz, Microstrip antenna, Stub and slot.

1. Introduction

The development of wireless communication systems has progressed rapidly to fulfil the growing requirement for improved connectivity. The fifth-generation (5G) mobile communication standards address these requirements through advanced multiple-input-multiple-output (MIMO) technologies, expanded spectrum allocation, and innovative antenna designs [1, 2]. The 5G New Radio (NR) standard supports operation in both sub-6 GHz and millimetre wave frequency bands [2].

Although millimetre wave bands enable high data rates due to their large bandwidth, their practical deployment is generally limited to short-range hotspots scenarios due to severe free-space path loss, high atmospheric absorption, and poor penetration capabilities [2, 3]. In contrast, the sub-6 GHz spectrum offers more favourable propagation characteristics, lower attenuation, and easier integration with existing cellular infrastructure, thereby supporting wide area 5G coverage.

Notably, a diverse array of hardware, including small-cell nodes, IoT sensors, and standard 5G handsets, heavily relies on specific mid-band allocations specifically n77, n78, and n79 for operational connectivity [4]. Consequently, antennas operating in these mid-band frequencies must be carefully designed to satisfy stringent size, performance, and integration constraints imposed by 5G terminals and network infrastructure.

Moreover, the capability to support dual-band operation is important to accommodate multiple 5G frequency allocations within the sub-6 GHz spectrum, improve spectral efficiency, and enhance network coverage. Such operation must be achieved while maintaining good impedance matching, stable radiation patterns, and minimal mutual coupling with surrounding components across all operating bands [5].

In the realm of 5G technology, microstrip topologies are a preferred solution, largely due to their negligible mass, low-profile geometry, and the ease with which they can be fabricated using standard printed circuit board workflows [6, 7]. These antennas can be readily integrated into compact embedded modules as well as larger platforms such as small-cell base stations and wireless terminals.

Typically, microstrip antennas operate at a single frequency band by exciting the fundamental TM_{10} mode, using microstrip antennas dimensions and substrate properties the resonate frequency is primarily determined [7, 8]. Single-band microstrip antennas for sub-6 GHz 5G applications have been extensively studied focusing on bandwidth enhancement, improved radiation efficiency, and impedance matching [6, 8].

However, a major limitation of conventional single-band antenna designs is their inability to simultaneously support multiple frequency bands, which is a critical requirement in 5G mobile communication system [9]. Multi-standard compatibility can be achieved while maintaining structural simplicity by transforming a single-band antenna into an optimally tuned multi-band antenna. Figure 1 depicts commonly used rectangular microstrip antenna structure which consists of a ground plane, a dielectric substrate, and a rectangular patch.

The literature has explored numerous design approaches to achieve dual-band or multi-band operation. Common techniques include stacked patches [8], parasitic element coupling [8], defected ground structures [10], and slotted radiators [7].

Although these techniques can enhance bandwidth and enable multi-band operation, they often result in increased antenna size, complex fabrication processes, and unwanted electromagnetic coupling. In recent years, single-layer approaches have gained attention for achieving dual-band operation without increasing antenna dimensions, demonstrating the effectiveness of stub and slot loading techniques [11].

Stub loading introduces additional resonant modes by modifying the surface current paths through conductive extensions attached to the microstrip antenna or feed microstrip transmission line, typically with quarter- wavelength [11, 12]. In contrast, slot loading introduces controlled perturbations in the microstrip antenna and ground plane to excite additional resonant modes and enhance bandwidth [7, 8]. These techniques offer cost-effective, planar, and low-profile solutions that are well suited for compact antenna integration in sub-6 GHz 5G applications.

Despite significant advancements, many reported dual-band antenna designs continue to face challenges in sub-6 GHz 5G applications [13]. Layered or stacked configurations increase fabrication complexity and high fabrication cost [10]. Furthermore, parasitic coupling and inverted-F antenna designs are often incompatible with compact devices due to their larger physical dimensions [13].

In addition, defected ground structure-based antennas may suffer from unwanted back radiation [11]. Several slot-based antenna designs employ non-optimized geometries or high-loss substrates, leading to radiation pattern instability and reduced antenna gain [7, 8]. These limitations highlight the need for a compact, single-layer dual-band microstrip antenna that provides high antenna gain, stable broadside radiation patterns across the sub-6 GHz 5G frequency bands.

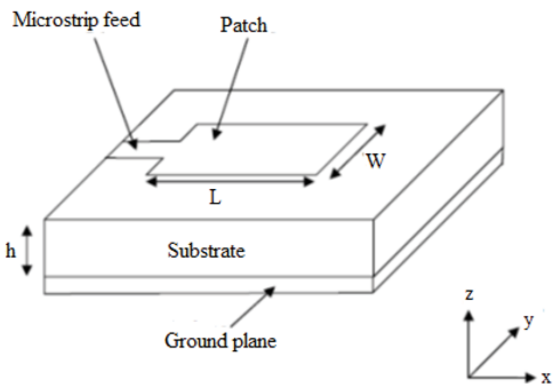

Fig. 1. Structure of rectangular microstrip antenna [14].

Furthermore, this paper outlines excitation of the fundamental TM_{10} mode using transmission-line model equations for the design of a single-band microstrip antenna operating at 3.6 GHz resonance. In order to achieve dual-band operation at 3.6 GHz and 5.4 GHz resonances, the single-band microstrip antenna is than modified using stub loading and slot loading techniques. These techniques enable dual-band operation while maintaining a compact antenna structure.

CST Studio Suite software is used for designing and simulation of the single band and the dual band microstrip antenna. The geometrical parameters of the antennas are optimized through parametric analysis to achieve optimal antenna performances. Simulated performance metrics for both the mono-band and dual-band antenna prototypes are reported and analysed.

2. Methods

Presented herein are the design strategies for a 3.6 GHz microstrip antenna, along with the modification techniques applied to induce a secondary resonance at 5.4 GHz, thereby enabling dual-band functionality suitable for sub-6 GHz 5G use. The procedure of the design begins with the calculation of the single-band microstrip antenna dimensions using transmission-line model equations. To achieve dual-band operation, a stub loading technique is first applied on the of the single-band microstrip antenna structure to introduce a second resonant mode, followed by a slot loading technique to fine-tune the second resonance at 5.4 GHz.

A low-loss NPC-F22A material was selected as the substrate for the single-band and dual-band microstrip antennas, featuring a dielectric constant of 2.2, a loss tangent of 0.0007, and a substrate height of 0.254 mm. Three-dimensional electromagnetic simulations are performed using CST Studio Suite software, and parametric optimization is carried out by refining the antenna dimensions to achieve optimal antenna performances.

2.1. Design of the single-band microstrip antenna

The primary design objective for the mono-band radiator is to establish resonance at 3.6 GHz by exciting the dominant TM_{10} cavity mode. The single-band microstrip antenna dimensions are initially calculated using transmission-line model equations. Using Eq. (1) the width of the single-band microstrip antenna, W_p is determined [6]:

$$W_p = \frac{c}{2f_r}\sqrt{\frac{2}{\varepsilon_r+1}} \tag{1}$$

In this expression, c denotes the speed of light in vacuum, ε_r represents the substrate's relative permittivity, and f_r corresponds to the resonant frequency.

Since the electromagnetic wave propagates partly in the surrounding air and partly in substrate, an effective dielectric constant must be taken into consideration. Using Eq. (2) the effective dielectric constant, ε_{eff} is calculated [6]:

$$\varepsilon_{eff} = \frac{\varepsilon_r+1}{2} + \frac{\varepsilon_r-1}{2}\left(1 + 12\frac{h}{W_p}\right)^{-\frac{1}{2}} \tag{2}$$

In this equation, h refers to the thickness of substrate.

The extension of electromagnetic fields beyond the patch boundaries causes the antenna's effective electrical footprint to exceed its actual physical geometry. Using Eq. (3) the effective length of the single-band microstrip antenna, L_{eff} is given [6]:

$$L_{\text{eff}} = \frac{c}{2f_r\sqrt{\varepsilon_{\text{eff}}}} \tag{3}$$

Using Eq. (4) the extended length of the single-band microstrip antenna, ΔL is calculated [6]:

$$\Delta L = 0.412h \frac{(\varepsilon_{\text{eff}}+0.3)\left(\frac{W_p}{h}+0.264\right)}{(\varepsilon_{\text{eff}}-0.258)\left(\frac{W_p}{h}+0.8\right)} \quad (4)$$

Using Eq. (5) the actual physical length of the single-band microstrip antenna, L_p is obtained [6]:

$$L_p = L_{\text{eff}} - 2\Delta L \quad (5)$$

The parameters which are calculated for the single-band microstrip antenna based on transmission-line model equations are listed in Table 1. These calculated dimensions serve as the starting point for the design workflow within CST Studio Suite. To ensure the radiator achieves peak efficiency, the model undergoes iterative simulation and fine-tuning. Figure 2 depicts the finalized structure featuring an inset feed, while Table 2 itemizes the specific geometric values post-optimization.

Table 1. Preliminary geometric specifications for the mono-band radiator.

Parameter	Value
$\boldsymbol{Wp}$	29.6 mm
$\boldsymbol{\varepsilon_{eff}}$"	2.07
$\boldsymbol{\Delta L}$	0.40 mm
$\boldsymbol{L_{eff}}$"	28.9 mm
$\boldsymbol{Lp}$	28.1 mm

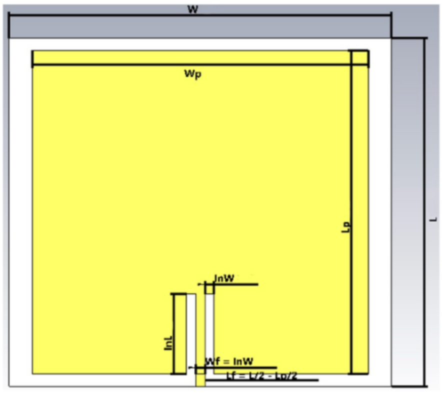

Fig. 2. Geometric configuration of the single-frequency patch radiator.

Table 2. Optimized parameters of the single-band microstrip antenna.

Parameter	Value (mm)
$\boldsymbol{W}$	33
$\boldsymbol{L}$	30
$\boldsymbol{W_p}$	29
$\boldsymbol{L_p}$	27.87
$\boldsymbol{W_f}$	0.78262
$\boldsymbol{Lf}$	1.065
$\boldsymbol{InL}$	6.9
$\boldsymbol{Inw}$	0.78262

2.2. Development of the two-band microstrip element antenna

The modification of the single-band microstrip antenna has occurred by incorporating a quarter-wavelength (λ/4) stub and half-wavelength (λ/2) slots to achieve dual-band operation. As illustrated in Fig. 3, a λ/4 stub is positioned at the top centre of the single-band microstrip antenna to introduce a second resonance TM_{11} mode at 5.4 GHz. By incorporating the stub, the current paths on the microstrip antenna are reconfigured, which redirects the radiation pattern at the second resonance toward boresight [7, 11, 12]. The length of the quarter wavelength stub, L_{stub} can be calculated using Eq. (6) [6, 7]:

$$L_{stub} = \frac{c}{4f_2\sqrt{\varepsilon_{eff}}} \quad (6)$$

where c is the free-space light velocity, the secondary resonant frequency f_2 equals 5.4 GHz, and $\varepsilon_{\mathrm{eff}}$ stands for the substrate's effective permittivity.

In addition to the λ/4 stub, two λ/2 slots are etched at the bottom centre of the single-band microstrip antenna near the inset-fed microstrip transmission line as shown in Fig. 3. These slots act as half-wavelength radiating elements that perturb the surface current distribution and contribute to the generation of a second resonance at 5.4 GHz. Using Eq. (7) length of the slot, L_{slot} can be determined [6, 7].

$$L_{slot} \approx \frac{\lambda_g}{2} = \frac{1}{2}\frac{c}{f_2\sqrt{\varepsilon_{eff}}} \quad (7)$$

where λ_g is the guided wavelength.

Furthermore, two-band microstrip element antenna has been optimized until optimal antenna performance is achieved. Table 3 depicts optimized values of two-band microstrip element antenna.

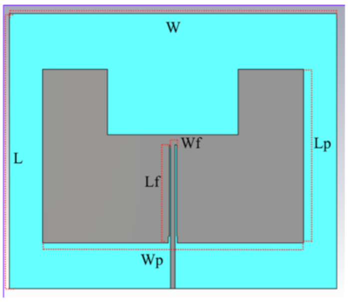

(a) Structure of the dual-band microstrip antenna.

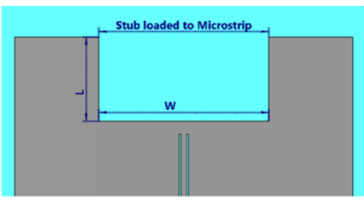

(b) Stub loaded.

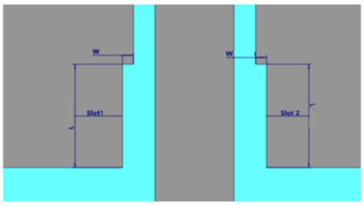

(c) Slot loaded.

Fig. 3. Structure of the two-band microstrip radiator.

Table 3. The optimized parameters of two-band microstrip radiator.

Parameter Symbol	Value (mm)
W	50
L	42
W_p	39.86
L_p	26.50
W_f	0.78262
L_f	7.75
L_{stub}	10
W_{stub}	10
L_{slot}	1.0
W_{stub}''	0.10

3. Results and Discussions

Sections 3.1 and 3.2 provide a comprehensive breakdown of the performance metrics observed for the mono-band and dual-resonance configurations, respectively.

3.1. Mono-band microstrip radiator

With the primary TM_{10} mode established at 3.6 GHz (see Section 2.1), this segment reports the simulation outcomes, highlighting both the scattering parameters and the directional characteristics of the mono-band element.

3.1.1. Return loss

Figure 4 highlights the spectral performance of the initial design, demonstrating a primary resonance magnitude of −20 dB at the centre frequency. The structure maintains acceptable matching (< −10 dB) across a 100 MHz span (3.55–3.65 GHz). In addition to scattering parameters, the corresponding real and imaginary impedance values are visualized in Fig. 5. The real and imaginary parts of the impedance at 3.6 GHz is 50 Ω and −2 Ω, respectively. These results indicate good impedance matching between the microstrip transmission line and the microstrip antenna.

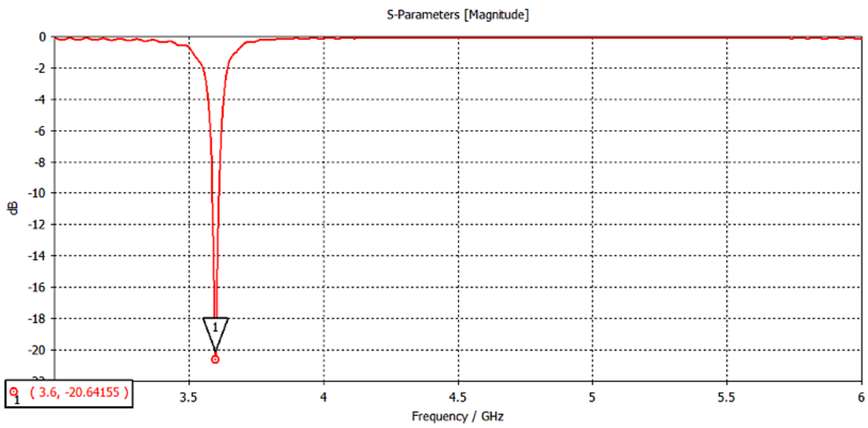

Fig. 4. Reflection coefficient characteristics of the mono-band element.

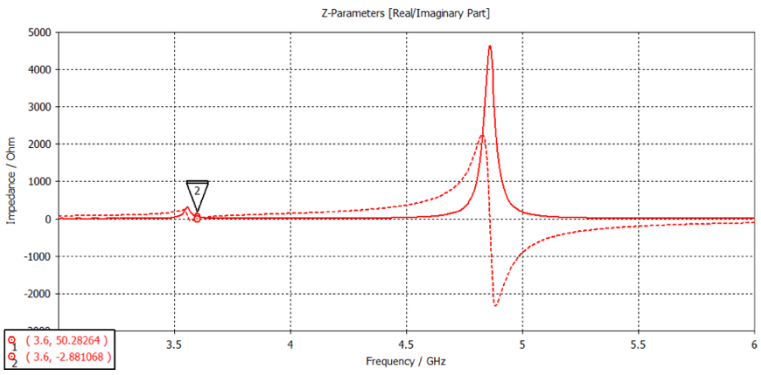

Fig. 5. Input impedance profile for the proposed single-frequency design.

3.1.2. Radiation characteristics

Figure 6 delineates the 2D far-field emission profiles for the 3.6 GHz element, specifically along the principal phi = 0° and phi = 90° cuts. As the data indicates, the radiator maintains a highly symmetrical distribution in the broadside direction, culminating in a peak gain of 7 dBi. To provide a complete spatial perspective, the corresponding volumetric (3D) radiation topology is mapped in Fig. 7.

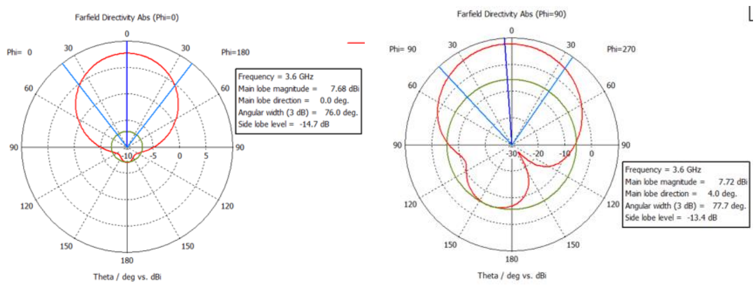

(a) Phi = 0°. **(b) Phi = 90°.**

Fig. 6. Radiation patterns of the single-band microstrip antenna at 3.6 GHz.

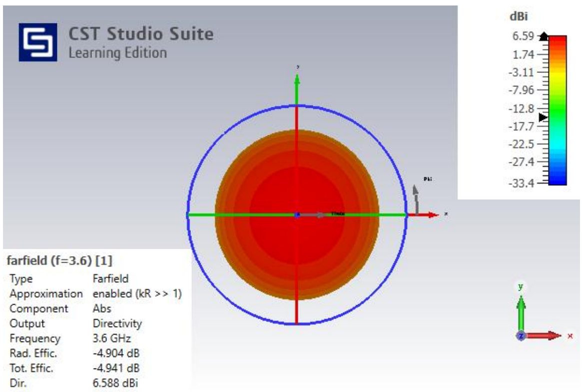

Fig. 7. Three-dimensional radiation pattern of the single-band microstrip antenna.

3.2. Results of the dual-band microstrip antenna

Consistent with the design objectives outlined in Section 2.2, the modified structure is engineered to support dual-frequency operation at 3.6 GHz and 5.4 GHz. The subsequent analysis validates this performance through simulation, specifically detailing the reflection coefficients (S_{11}) and far-field emission properties of the proposed radiator.

3.1.3. Return loss

Figure 8 depicts S_{11} profile for the proposed dual-frequency structure. The plot reveals two distinct resonant modes: a primary dip of −35.1 dB at 3.6 GHz and a secondary dip of −13.7 dB at 5.4 GHz. Furthermore, both bands maintain an impedance matching level below −10 dB across the 3.55–3.65 GHz and 5.35–5.45 GHz frequency ranges.

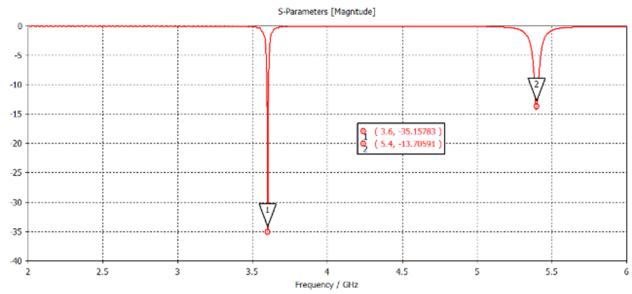

Fig. 8. Reflection coefficient profile of the two-frequency radiator.

3.1.4. Radiation characteristics

Figures 9 and 10 present the radiation patterns of the dual-band microstrip antenna at 3.6 GHz and 5.4 GHz resonances for Phi = 0° and Phi = 90°, respectively. As shown in the figures, the resulted radiation patterns of the simulated dual-band microstrip antenna at the boresight exhibit good symmetry. The resulted gain of the antenna for Phi = 0° and Phi = 90° are 7.77 dBi and 6.4 dBi at 3.6 GHz and 5.4, respectively. The three-dimensional radiation patterns of the dual-band microstrip antenna are presented in Fig. 11.

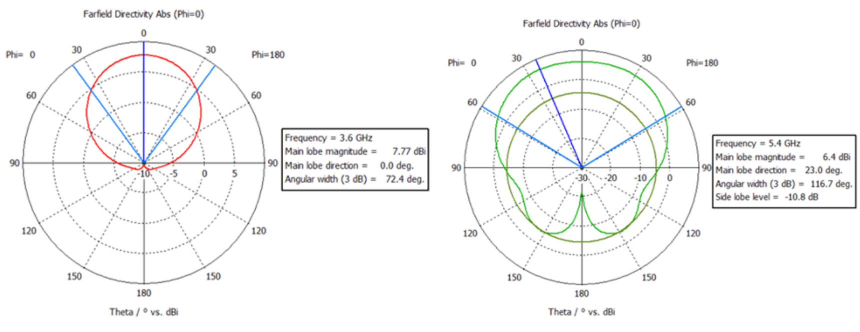

(a) 3.6 GHz. **(b) 5.4 GHz.**

Fig. 9. Radiation patterns of the dual-band microstrip antenna for Phi = 0°.

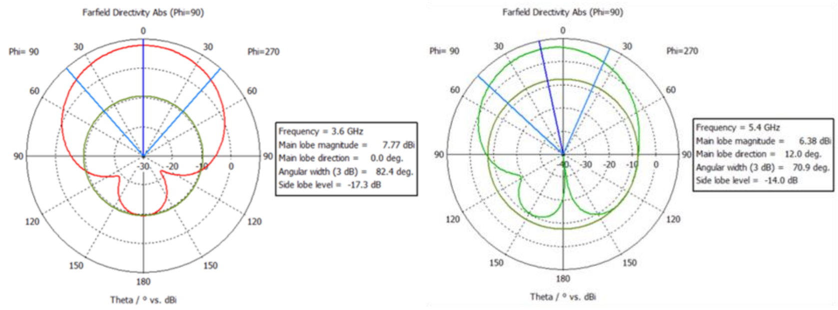

(a) 3.6 GHz. (b) 5.4 GHz.

Fig. 10. Radiation patterns of the dual-band microstrip antenna for Phi = 90°.

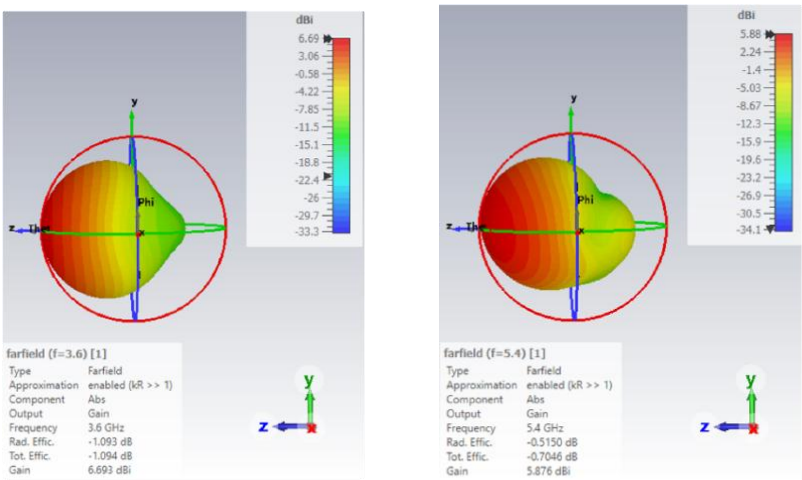

(a) 3.6 GHz. (b) 5.4 GHz.

Fig. 11. Three-dimensional radiation patterns of the dual-band microstrip antenna.

3.3. Comparative analysis of the developed two-band element versus existing solutions

Table 4 provides a concise benchmarking analysis, contrasting the performance metrics of our dual-resonance design against established solutions found in recent literature. In comparison to the previous works, the developed two-band element resulted in higher antenna gains at both operating frequencies by employing a low-loss substrate, which reduces dielectric losses and enhances the antenna gains. In contrast, the antenna designs reported in [15, 16] results in lower antenna gains due to the utilization of FR-4 substrate which has high dielectric constant.

Furthermore, the proposed dual-band microstrip antenna employs a simple stub and slot loading techniques without introducing structural complexity, such as defected ground structures [17, 18] and parasitic strips [11], which increase fabrication complexity and may generate unwanted back radiation and electromagnetic coupling. Therefore, two-band microstrip antenna presented in this paper demonstrates an assuring solution for sub-6GHz 5G applications.

Table 4. Comparative results between proposed and previous works.

Ref.	Centre Frequency (GHz)	Substr-ate material	Dielectric constant	Tan-gent loss	Antenna Gain (dBi)	Size (mm^3)
[15]	3.6 5.4	FR-4	4.4	0.02	1.0 2.2	36 × 37 × 1.635
[17]	4.53 4.97	Rogers 5880	2.2	0.0009	5 4.57	77 × 70.1 × 1.635
[18]	3.12	Rogers 5880	2.2	0.0009	4.65	20 × 35 × 0.79
[11]	3.4 5.9	FR-4	4.3	0.02	3.83 0.537	36 × 37 × 1.635
This work	3.6 5.4	NPC-F220A	2.2	0.0007	6.7 5.87	50 × 42 × 0.289

4. Conclusions

In this paper, a single-band microstrip antenna design operating at 3.6 GHz and a dual-band microstrip antenna design operating at 3.6 GHz and 5.4 GHz, based on single-layer structure are outlined for 5G applications in sub-6 GHz. The initial design of the single-band microstrip antenna is obtained using transmission-line model equations to determine the length and width of the single-band microstrip antenna.

The dual-band operation is realized by first introducing a stub-loading technique to generate a second resonance around 5.4 GHz, followed by a slot-loading technique to fine-tune the second resonance frequency. Using these methods, the design operates on both 3.6 GHz and 5.4 GHz bands without increasing footprint. The finished dual-band microstrip measures $50 \times 42 \times 0.289\, mm^3$ confirming a compact form factor suitable for implementation. A low-loss NPC-F220A substrate with a low dielectric constant and a low tangent loss is used to design the antenna.

Simulation analysis revealed that the dual-resonance structure achieves reflection coefficients of −35.7 dB at 3.6 GHz and −13.7 dB at 5.4 GHz. Correspondingly, the design delivers peak gains of 7.77 dBi and 6.4 dBi for the respective frequencies. Furthermore, the radiation patterns maintain excellent symmetry in the broadside direction across both bands. These performance indicators confirm the antenna's suitability for Sub-6 GHz 5G applications. The next phase of research will prioritize the physical fabrication of the prototype to experimentally validate these computational findings.

Acknowledgement

The authors gratefully acknowledge the financial assistance provided by Taylor’s University, Malaysia, under the Taylor’s Internal Research Grant Scheme-Impact Lab Grant (Grant No. TIRGS-ILG/2/2024/SOE/002).

References

1. Akyildiz, I.F.; Nie, S.; Lin, S.-C.; and Chandrasekaran, M. (2016). 5G roadmap: 10 key enabling technologies. *Computer Networks*, 106, 17-48.
2. Andrews, J.G.; Buzzi, S.; Choi, W.; Hanly, S.V.; Lozano, A.; Soong, A.C.K.; and Zhang, J.C. (2014). What will 5G be? *IEEE Journal on Selected Areas in Communications*, 32(6), 1065-1082.

3. Oladimeji, T.T.; Kumar, P.; and Oyie, N.O. (2022). Propagation path loss prediction modelling in enclosed environments for 5G networks: A review. *Heliyon*, 8(11), e11581.
4. GPP. (2018). New frequency range for NR (3.3-4.2 GHz). TR 38.813 (Release 15). 3rd Generation Partnership Project.
5. Dahlman, E.; Parkvall, S.; and Sköld, J. (2020). 5*G NR*: *The Next Generation Wireless Access Technology*. Academic Press, Elsevier. 3
6. James, J.R.; and Hall, P.S. (1989). *Handbook of Microstrip Antennas*. Inst of Engineering & Technology.
7. Balanis, C.A. (2016). *Antenna Theory*: *Analysis and Design* (4th *Edition*). John Wiley & Sons.
8. Garg, R.; Bhartia, P.; Bahl, I.; and Ittipiboon, A. (2001). *Microstrip Antenna Design Handbook*. Artech House.
9. Osseiran, A. et al. (2014). Scenarios for 5G mobile and wireless communications: The vision of the METIS project. *IEEE Communications Magazine*, 52(5), 26-35.
10. Weng, L.H.; Guo, Y.-C.; Shi, X.-W.; and Chen, X.-Q. (2008). An overview on defected ground structure. *Progress in Electromagnetics Research B*, 7, 173-189.
11. Noor, S.K.; Jusoh, M.; Sabapathy, T.; Rambe, A.H.; Vettikalladi, H.; Albishi, A.; and Himdi, M. (2023). A patch antenna with enhanced gain and bandwidth for sub-6 GHz and sub-7 GHz 5G wireless applications. *Electronics*, 12(12), 2555.
12. Bhatt, R.V.; and Makwana, G.D. (2024). Slot-loaded dual-band microstrip patch antenna for 5G and WLAN/WiMAX wireless applications. *Indian Journal of Science and Technology*, 17(22), 2324-2330.
13. Jibin, H.; and Yihang, H. (2019). A compact dual band antenna for TD-LTE/WiMAX applications. *Proceedings of the* 2019 *International Symposium on Signal Processing Systems*, Beijing, China, 67-71.
14. Paul, L.C.; Rashid, M.M.U.; Mowla, M.; Morshed, M.; and Sarkar, A.K. (2016). Performance analysis of cut feed rectangular microstrip patch antenna by varying feeder length and width. *Proceedings of the* 3rd *International Conference on Electrical*, *Electronics*, *Engineering Trends*, *Communication*, *Optimization and Sciences* (*EEECOS* 2016), Tadepalligudem, India.
15. Kadu, M.; Pawase, R.; Chitte, P.; and Ubale, V.S. (2024). Compact dual-band antenna design for sub-6 GHz 5G application. *Bulletin of Electrical Engineering and Informatics*, 13(3), 1656-1666.
16. Dassault Systèmes. (2026). CST Studio Suite: Electromagnetic field simulation software. Retrieved January 10, 2026, from https://www.3ds.com/products/simulia/cst-studio-suite.
17. Sree, M.F.A.; Elazeem, M.H.A.; and Swelam, W. (2021). Dual band patch antenna based on letter slotted DGS for 5G sub-6 GHz application. *Journal of Physics*: *Conference Series*, 2128(1), 012008.
18. Paul, L.C.; Das, S.C.; Rani, T.; Muyeen, S.M.; Shezan, S.A.; and Ishraque, M.F. (2022). A slotted plus-shaped antenna with a DGS for 5G Sub-6 GHz/WiMAX applications. *Heliyon*, 8(12), e12040.